International Journal of Science and Research Methodology (IJSRM)
Volume 29, Issue 6, June 2026 ijsrm.humanjournals.com ISSN: 2454-2008

Δ^9-THC, CBN, and CBD in Glaucoma: A Theoretical Insight in Light of Molecular Electrostatic Potential and CB1 and CB2 Ligand-Receptor Interaction

José Ciríaco Pinheiro[a, b], Antonio Florêncio de Figueiredo[c], Ana Cecília Barbosa Pinheiro[d], Marcos Antônio Barros dos Santos[e], Heriberto Rodrigues Bitencout[f], Andreia de Lourdes Ribeiro Pinheiro[g], Fábio dos Santos Gil[h], Marcos Daniel Gonçalves Pizon[a]

[a]Laboratório de Química Teórica e Computacional (LQTC), Universidade Federal do Pará (UFPA), Belém, PA, Brasil
[b]Instituto Amazônia dos Saberes (IASA), São Luís, MA, Brasil
[c]Laboratório de Solos e Plantas, Instituto de Federal de Educação Ciência e Tecnologia do Pará (IFPA), Castanhal, PA, Brasil
[d]Fundação Santa Casa de Misericórdia do Pará (FSCMPA), Belém, PA, Brasil
[e]Universidade do Estado do Pará, Belém, PA, Brasil
[f]Laboratório de Síntese Orgânica (LabSínt), Universidade Federal do Pará, Belém, PA, Brasil
[g]Centro Educa Mais Padre José Bráulio de Sousa Ayres (CEMPJB), São Luís, MA, Brasil
[h]Escola Estadual Rodrigues Pinagé (EERP), Belém, PA, Brasil

Received: 20 April 2026 Revised: 11 May 2026 Accepted: 23 May 2026

ABSTRACT

Initially, the molecular electrostatic potential (MEP) quantum chemistry approach was used to investigate the key structural features of the cannabinoids Δ^9-THC, CBN, and CBD in their interaction with CB1 and CB2 receptors in glaucomatous processes involving reduction (Δ^9-THC and CBN) or increase (CBD) in intraocular pressure (IOP), and also as modulators of the neuroprotective effects mediated by these receptors. Subsequently, the interactions of the cannabinoids Δ^9-THC, CBN, and CBD with CB1 and CB2 were investigated through molecular docking and molecular dynamics (MD). It can be noted that the lack of theoretical research on this topic in the literature makes this research the first insight of this nature to be made available in the literature.

Keywords: Δ^9-Tetrahydrocannabinol (Δ^9-THC); Cannabinol (CBN); Cannabidiol (CBD); Glaucoma; Molecular electrostatic potential; CB1 and CB2 ligand-receptor interaction

INTRODUCTION

According to the literature, glaucoma is one of the leading causes of blindness worldwide and is characterized by the progressive deterioration and loss of function of retinal ganglion neurons with optic nerve degeneration [1, 2]. Statistics are not updated, but for the year 2020, the forecast was 76 million cases, with 4.5 millions of that total associated with moderate visual impairment and 3.2 millions with total vision loss. Additionally, a projection of 112 millions prevalent cases was established for 2040 [3]. Also according to the literature, one of the most important factors in the onset of glaucoma and in the progression of the disease is the increase in IOP, with studies reporting ocular hypotension as a factor also responsible for the progression of the disease [4].

The literature on the subject reports aqueous humor (AH) as a transparent fluid that maintains the integrity of the eye, being introduced through the ciliary body, passing through the trabecular meshwork (TM) and Schlemm's canal. IOP is determined by the amount of aqueous humor secreted, along with the eye's clearance rate. Elevated IOP leads to optic nerve deterioration and irreversible functional vision loss [5, 6]. The balance between AH secretion by the ciliary bodies and its drainage via TM and uveoscleral flow is essential to maintain ideal IOP in the eyes. In glaucoma, this balance is disturbed by excessive production or reduced AH flow, resulting in increased IOP [7].

Cannabinoids are classified into three categories, as follows. Phytocannabinoids: substances collected from the leaves, flowers, stems, seeds of Cannabis Sativa and also from the resin secreted by the female plant [8], for example, Δ^9-Tetrahydrocannabinol (Δ^9-THC), cannabidiol (CBD), and cannabinol (CBN) etc.; endogenous cannabinoids: N-arachidonoyl ethanolamine (AEA), commonly known as Anandamide, and 2-arachidonoylglycerol (2-AG) etc.; and synthetic cannabinoids: JWH-133, WIN55,212-2 etc. Cannabinoids exert a broad spectrum of central and peripheral actions, such as: analgesia, anticonvulsants, anti-inflammatories, IOP relief etc. (An overview of the aspects of cannabinoid and Cannabis Sativa actions can be found in the References [9,10]). The manifestation of most pharmacological effects exhibited by cannabinoids is effected by the activation of at least one of the type 1

(CB1) and type 2 (CB2) G protein-coupled cannabinoid receptors [8-11]. The CB1 receptor is expressed in the brain, spinal cord, and certain peripheral tissues, including the lung, heart, urogenital and gastrointestinal tracts, and eye [12, 13], while the CB2 receptor is expressed mainly in peripheral tissues and the immune system [12, 13]. In the human eye, both CB1 and CB2 receptors are present in the retina, ciliary body, and retinal pigment epithelium.

The detection of the CB1 receptor in the human eye has been evidenced in the cornea, iris, ciliary body, including the epithelium, ciliary muscle and blood vessels of the ciliary body, TM, Schlemm's canal and retina [14,15]. According to the literature, the critical anatomical location and distribution of cannabinoid receptors indicate that this class of compounds can increase HA efflux or decrease HA production, influencing IOP [7,16-19]. Furthermore, the existence of the CB1 receptor in the TM and Schlemm's canal suggested a possible influence of these compounds on conventional HA flow [20], with HA production and/or uveoscleral flow producing an effect via the CB1 receptor in the ciliary pigment epithelium and ciliary muscle [20]. It has also been evidenced in the ganglion cell layer, the inner and outer plexiform layers, as well as the inner nuclear layer and outer segments of the retinal photoreceptors [14, 21]. In turn, in the human eye, the precise distribution and functions of the CB2 receptor appear to be poorly understood; however, it has been evidenced in the cornea, TM and retina [21-24], in cell layer types such as amacrine, bipolar, Müller, microglial and retinal ganglion cells (RGCs), or in the retinal pigment epithelium [13,22, 25-29]). Activation of the CB2 receptor has been associated with reduced inflammation and neuroprotection [7,29,30]. Evidence of the importance of CB1 and CB2 receptors in the functional modulation of neuroretinal cells in animal tissues makes them a potential target for neuroprotection [15,21].

Literature reports the functional importance of cannabinoids as an effective therapeutic approach to control and regulate IOP increases and promote neuroprotection in glaucoma pathogenesis [29]. Among the most studied phytocannabinoids are Δ^9-THC, CBD, and CBN [13]. While Δ^9-THC reduces IOP and has analgesic and neuroprotective effects – but is psychoactive – CBN, in addition to also reducing pressure and not being psychotropic, exerts sedative, analgesic, anti-inflammatory, and neuroprotective effects [7,13,31]. Regarding IOP, according to the literature, CBD has the opposite effect to the cannabinoids Δ^9-THC and CBN, but has sedative, anti-inflammatory, and neuroprotective properties, and is not psychotropic [15, 32-34].

In this article, initially, the MEP is used to investigate the key structural features of the cannabinoids Δ^9-THC, CBN, and CBD in their interaction with CB1 and CB2 receptors in glaucomatous processes where IOP reduction occurs (Δ9-THC and CBN through interaction with the CB1 receptor) or IOP increases (CBD through interaction with the CB1 receptor), and also as important modulators of signaling pathways in the neuroprotective mechanism mediated by these receptors (CB1 and CB2). Subsequently, the interactions of these cannabinoids with their respective receptors are investigated through molecular docking and molecular dynamics (MD).

The guiding principle of this investigation was to explore aspects of the interaction of the cannabinoids Δ^9-THC, CBN, and CBD with the CB1 receptor in the eye regions where glaucomatous processes associated with IOP occur, with all their complexity, and with the CB1 and CB2 receptors in the eye regions where neuroprotective effects develop. It can be noted that the lack of theoretical research on this topic in the literature makes this research the first insight of this nature to be reported.

2 METHODOLOGY

2.1 A Brief Overview of the Mechanisms by which Cannabinoids Reduce Intraocular Pressure and Their Neuroprotective Effects

2.1.1 Mechanisms for Reducing Intraocular Pressure

According to the literature, cannabinoids can influence intraocular pressure by reducing HA production in the ciliary muscle and increasing HA flow [2, 4, 7, 15, 35, 36] through the TM and Schlemm's canal [4, 7, 35], as well as modifying cyclooxygenase-2 activity [35, 37]. These mechanisms depend on interaction with the CB1 receptor and modulation of the cyclooxygenase pathway and prostanoid synthesis [20, 35]. Therefore, since cannabinoids have the ability to regulate HA synthesis and flow, they may constitute an effective therapeutic alternative in the treatment of glaucoma by reducing IOP [29].

2.1.2 Neuroprotective Effects of Cannabinoids

Cannabinoids exhibit neuroprotective effects in the pathogenesis of glaucoma through various mechanisms, such as the inhibition of the toxic effects of glutamate, nitric oxide (NO), and endothelin-1, associated with the degeneration of retinal ganglion cells. Glutamate, being neurotoxic, can accelerate damage to the optic nerve [7]. According to the literature, the protection of ganglion cells from degradation produced by this neurotransmitter results from the activation of CB1 and CB2 receptors that act to reduce its release [35]. Additionally, cannabinoids act by inhibiting the production of NO and inflammatory cytokines, reducing oxidative stress and therefore protecting retinal ganglion cells [2]. Furthermore, activation of CB1 and CB2 receptors induces the vasodilatory

properties of cannabinoids, neutralizing the effects of endothelin-1, increasing blood flow to the optic nerve head and reinforcing its neuroprotective effects in glaucoma [36]. In addition, its anti-inflammatory properties contribute to the protection of retinal nerve cells [15].

2.2 Computational Details

The starting point of the computational approach was the visualization with the MOLDEN 6.3 program [38] of the 3D structure of the cannabinoid Δ^9-THC, whose complete optimization was reported by Cardoso et al. [39]. This structure was then used as a basis for the construction of the 3D structures of the cannabinoids CBN and CBD, respectively, with the aid of the HYPERCHEM 8.06 program [40], after conversion by the OPENBABEL 3.1.0 program [41]. The 3D structures of the cannabinoids were also subjected to complete optimizations with the GAUSSIAN 98 program [42] using the B3LYP/6-31G* approximation of Becker [43], Lee et al. [44], and Hehre et al. [45] reported by Cardoso-Filho et al. [39] as the most promising in describing the most stable conformation of the cannabinoid environment. Figure 1 shows the 2D (Figures 1a to 1c) and 3D (Figures 1d to 1f) structures of the cannabinoids Δ^9-THC, CBN, and CBD, which are the subject of this investigation. Figure 1a shows the atomic numbering used in this study. In this figure, the phenolic OH group at position C1, the alkyl (lipophilic) side chain at position C3, and the carbocyclic ring system (rings A and C) are noted, which, according to Tomas et al. [46], when appropriately oriented, are essential in defining the pharmacophoric conformation necessary for the pharmacological properties of phytocannabinoids. In the most stable conformation (lowest energy), for THC, CBN, and CBD (Figures 1d to 1f), the electrostatic potential $V(\vec{r})$ was obtained at a point r with the given equation, namely [47]:

$$V(\vec{r}) = \sum_{A} \frac{Z_A}{|\vec{R}_A - \vec{r}|} - \int \frac{\rho(\vec{r}')d\vec{r}'}{|\vec{r}' - \vec{r}|} \qquad (1)$$

with Z_A representing the charge of the nucleus A located in $\vec{R}_A$ and $\rho(\vec{r}')$ being associated with the electron density of the molecule; $V(\vec{r})$ in a given region will depend on the positive and negative contributions of the nuclei and electrons, respectively [48]. The MEPs were obtained with the electron densities and visualized with the MOLEKEL program [49].

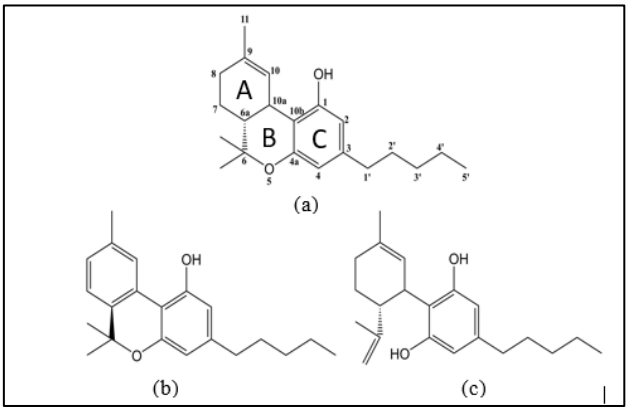

Figure 1. 2D structure of the cannabinoids Δ^9-THC (with numbering), CBN, and CBD.

A machine containing OPENSUSE LINUX 11.0 environment, 64-bit, AMD PHENOM 955X4, 2.2 GHZ processor, and 4 GB of RAM was used to produce the quantum chemistry calculations.

In the investigation of ligand-receptor interactions, the structures of the CB1 and CB2 complexes were obtained from the Protein Data Bank (RCSB-PDB) [50] under accession codes 9ERX [51] and 8GUS [52] with resolutions of 2.90 and 2.97 Å, respectively (Figure 2; see receptor architecture in the cited references). For both receptors, the proteins were prepared by using the UCSF CHIMERAX v1.10.1 program [53], with the removal of endogenous ligands, water molecules and addition of hydrogen atoms with the DOCKPREP tool, integrated into the program itself. Molecular docking calculations were performed with the AUTODOCK-GPU v1.6 program [54]. Two cubic search boxes with sides of 50 Å were defined, centered on the coordinates of the CB1 and CB2 receptor binding sites x = 131.353 and 130.005; y = 132.721 and 121.791; z = 163.530 and 170.767, respectively, with a grid spacing of 0.375 Å. 1,000 poses were generated for each ligand. The selection of the initial pose for the MD simulations was based on combined criteria: (i) lowest binding free energy; (ii) distance between relevant hydrogen bond donors/acceptors; and (iii) proximity between aliphatic carbon atoms of the ligand and the TRP279 residue of the CB1 receptor and TRP194 of the CB2 receptor, conserved structural markers in the active sites. The poses that best met these criteria were chosen as starting structures for subsequent MD simulations.

MD simulations were performed by using the GROMACS 2024.4 package [55], with the CHARMM36 force field [56, 57]. The initial structure of the protein-ligand complex was prepared by using the CHARMM-GUI program [58], which generated topological and coordinate files compatible with the CHARMM protocol, including the appropriate protonation of residues at physiological pH, parameterization of the ligand based on the charges and parameters of the CGENFF program [59]. The system was inserted into a dodecahedral box with TIP3P water, maintaining a minimum distance of 1.2 nm between any atom of the complex and the edge of the box. A concentration of 0.15 M NaCl was used to ensure the physiological conditions of the system, with the total charge of the system neutralized with Na^+ and Cl^- ions. Energy minimization was conducted in two stages. Initially, the steepest descent algorithm was employed with a force tolerance of 1000 $kJ•mol^{-1}•nm^{-1}$. Subsequently, a more rigorous minimization was performed with a tolerance of 200 $kJ•mol^{-1}•nm^{-1}$, using the same algorithm and positional constraints applied to both the protein and the ligand. The system was subjected to an equilibration step in an NVT ensemble (1 ns, 300 K) with a V-rescale thermostat. Next, equilibration was performed in an NPT ensemble, with pressure controlled at 1 bar by the Parrinello-Rahman barostat and isotropic coupling. The production simulation lasted 500 ns, with an integration step of 2 fs. Bonds involving hydrogen atoms were restricted by the LINCS algorithm. Van der Waals interactions were treated with a cutoff of 1.2 nm, with the switch function initiated at 1.0 nm. Long-range electrostatic interactions were calculated using the Particle Mesh Ewald (PME) method, with a grid spacing of 0.16 nm and cubic interpolation order (4th order). During the production simulation, coordinates were saved every 10 ps for later analysis.

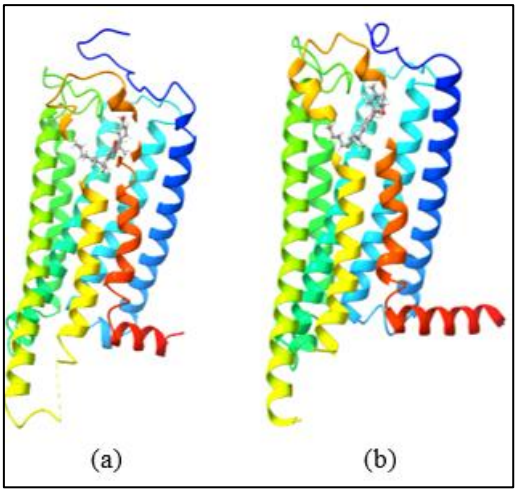

Figure 2. Structure of (a) the HU210-CB1 complex and (b) the AM12033-CB2 complex. The ligand structures are highlighted in ball and stick format.

The trajectories of the molecular dynamics simulations were analyzed in terms of root mean square deviation (RMSD) and root mean square fluctuation (RMSF). After the simulations were completed, 500 equally spaced snapshots were extracted from the complete trajectory by using the gmx trjcat tool of the GROMACS 2024.4 program, aiming at detailed structural analyses. Binding energies were calculated directly from the simulations by using the gmx mdrun module, based on the parameters of the CHARMM36 force field. The visualization of representative poses was performed by using the UCSF CHIMERAX v1.10.1 program. The identification and quantification of hydrophobic contacts and hydrogen bonds were automated by using custom scripts developed in Python, with the help of the Biophyton package for structural processing. RMSD and RMSF plots were generated by using the Matplotlib program.

3 RESULTS AND DISCUSSION

3.1 MEP maps for the cannabinoids Δ^9-THC, CBN, and CBD

Preliminarily, before presenting and discussing the MEP results for Δ^9-THC, CBN, and CBD, some considerations regarding molecular requirements indicated by traditional structure-activity relationships for cannabinoid activity are listed. These requirements include: (1) the phenolic OH group at C1, (2) the lipophilic side chain ($-CH_2-CH_2-CH_2-CH_2-CH_3$) at C3, and (3) a properly oriented carbocyclic ring system (A and C) [46]. In light of the highlighted requirements, the structures of Δ^9-THC, CBN, and CBD fit perfectly. CBD, lacking ring B, maintains a highly flexible A and C ring system around the C10a-C10b linkage. CBN exhibits greater rigidity in the orientation of its ring system due to the aromaticity of ring A (benzene ring), in contrast to Δ^9-THC and CBD, in which ring A is a cyclohexene. This difference likely results in a conformation that influences its orientation in the interaction with the CB1 receptor, which may favor the absence of psychopharmacological activity in CBN. Additionally, the lack of ring B in CBD confers greater molecular flexibility (ring system A and C) around the C10a-C10b linkage, as mentioned. Consequently, this may lead to a conformation whose orientation, when interacting with the CB1 receptor, is unfavorable to the

manifestation of psychoactivity in this cannabinoid. On the other hand, the presence of all three molecular requirements, including ring B, in the cannabinoids Δ^9-THC and CBN, suggests that the acquired conformations provide the desirable orientation of the ring system in interactions with the CB1 receptor. Thus, they contribute to the mechanism of IOP reduction. In contrast, the absence of this ring in CBD may lead to an inadequate interaction with the aforementioned receptor, not resulting in a reduction in IOP or, potentially, favoring its increase. Regarding the neuroprotective properties of the three cannabinoids, mediated by interactions with CB1 and CB2 receptors, the phenolic OH group at C1, the side chain at C3, and the orientation of the carbocyclic ring system (A and C) appear to be crucial for these activities. Additionally, Δ^9-THC, CBN, and CBD can interact with the body's endocannabinoid system, modulating pain and inflammation at multiple physiological levels [60] and exhibiting most of their pharmacological effects through G protein-coupled CB1 and CB2 receptors [11], as mentioned in the Introduction.

Considering the previous observations, Figures 3a to 3c show the MEP maps for the cannabinoids Δ^9-THC, CBN, and CBD, respectively. According to these figures, the three cannabinoids exhibit a similar pattern of electron density distribution, with MEP values ranging from -94.13 to +228.8 kcal/mol, where these values correspond to the regions of the maps represented in red, yellow, green, and blue. The highest electron densities are distributed in the range of $V(\vec{r})$ = -94.13 kcal/mol (red) to $V(\vec{r})$ = -11.17 kcal/mol (yellow), while the lowest densities occur between $V(\vec{r})$ = +55.79 kcal/mol (green) and $V(\vec{r})$ = +228.13 kcal/mol (blue). Furthermore, the distribution pattern of higher electron density for the cannabinoid Δ^9-THC (Figure 3a) is concentrated in the MEP range of -89.11 to -11.17 kcal/mol; while for the cannabinoid CBN (Figure 3b), this pattern is evident in the MEP range of -87.22 to -15.62 kcal/mol, and covers the MEP range of -99.13 to -15.00 kcal/mol for the cannabinoid CBD (Figure 3c).

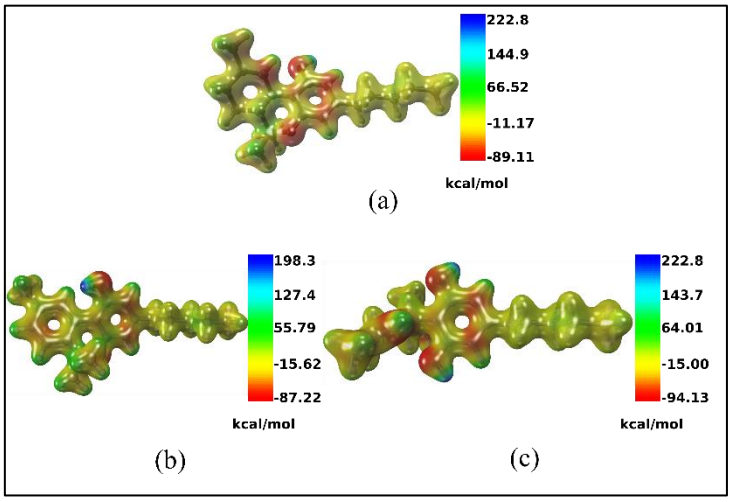

Figure 3. MEP (kcal/mol) maps for the cannabinoids Δ^9-THC, CBN, and CBD.

In Figure 3a, the highest electron densities are located at the oxygen atoms of the phenolic OH group (most intense red color, $V_{min}(\vec{r})$ = -89.11 kcal/mol), at C10 of ring A (sp^2 unsaturation), at the CH_3 branches in C6, at the O5 atom of ring B, at the C2, C4, and C10b atoms of the phenolic ring, and at C11 (branch in C9). Other atoms, with regions of intermediate electron density, correspond to carbons C6a, C7, C8 (all present in ring A) and C1', C3', and C5' (alkyl chain). Regarding the MEP map of this cannabinoid, it is possible to highlight that the MEP values, the presence of the phenolic OH group at C1, the side chain at C3, and the orientation of the carbocyclic ring system (rings A and C), indicate the existence of key structural characteristics in the cannabinoid Δ^9-THC. These characteristics enable interactions with CB1 and CB2 receptors, indicating its relevance in reducing IOP (interaction with the CB1 receptor), in neuroprotection (via CB1 and CB2 receptors), and in pain modulation (analgesic action). It is also worth noting that the psychoactivity of this cannabinoid possibly stems from these key structural characteristics in the interaction with the CB1 receptor.

In CBN, the highest electron density is located on the oxygen atom of the phenolic OH group with $V_{mín}(\vec{r})$ = -87.22 kcal/mol. Other high-density regions are located on the carbon atoms of the branches at C6, on O5 of ring B, on atoms C4, C2, and C10b of the phenolic ring, on C11 (branch at C9), on C7, C8, and C10 of the benzene ring (ring A), and on C5' of the alkyl chain. Moderate electron densities are observed on the alkyl carbons C1', C2', and C3'. In this cannabinoid, ring B is positioned relative to ring C differently from its positioning in Δ^9-THC, which likely influences the orientation of its carbocyclic ring system. In this case, the presence of the phenolic OH at C1, the side chain at C3, the orientation of the carbocyclic ring system combined with the $V(\vec{r})$ values show that the cannabinoid CBN has key structural characteristics that enable interactions with CB1 and CB2 receptors, justifying its relevance in reducing IOP (interaction with the CB1 receptor), in exerting sedative, analgesic, anti-inflammatory and neuroprotective effects (interaction with CB1 and CB2 receptors), with the absence of psychotropic properties probably resulting from these key structural characteristics in the interaction with the CB1 receptor.

In the cannabinoid CBD, according to the MEP map (Figure 3c), the breaking of the O5-C6 bond of ring B results in an increase in electron density at the O5 atom (region of highest electron density with $V_{mín}$ ($\vec{r}$) = -94.13 kcal/mol). The O1 atom of the OH group of resorcinol has an electron density similar to C10 of ring A (sp^2 unsaturation), with values slightly lower than the density at O1. Other relevant densities are found on the C atom of the CH_3 proximal to O5, on C2 and C4 of resorcinol, and C11 of ring A. Moderate densities are found on the C atoms of the branch distal to O5, C6a, C7, and C8 of ring A, C10a of resorcinol, and C1', C3', and C5' of the alkyl chain. For the cannabinoid CBD, the presence of the phenolic OH at C1, the side chain at C3, the proper orientation of the carbocyclic ring system combined with the V($\vec{r}$) values show that it has key structural characteristics that enable interactions with CB1 and CB2 receptors, and lead to the manifest absence of IOP reduction (interaction with the CB1 receptor), justifying its sedative, analgesic, anti-inflammatory and neuroprotective effects (interaction with CB1 and CB2 receptors). The absence of psychotropic properties is likely also due to these key structural characteristics in the interaction with the CB1 receptor.

3.2 Interactions of the Main Cannabinoid Fragments Δ^9-THC, CBN, and CBD with the CB1 Receptor

Figure 4 shows the ligand-CB1 receptor interactions. Figure 4a shows the analyzed poses of Δ^9-THC (purple), CBN (yellow), and CBD (blue), and Figures 4b to 4d show the interactions of the main cannabinoid fragments with the CB1 receptor. According to this figure, the ligands establish conserved hydrophobic interactions between their alkyl chains and three key residues of the CB1 receptor's active site, namely TRP279, PHE200, and LEU276, which form a fundamental hydrophobic core for the stabilization of the ligand-protein complexes. The MET363 residue participates in interactions with all ligands, but with less intensity compared to the three main residues, suggesting an auxiliary role in molecular stabilization. The ILE280 residue selectively interacts with the cannabinoids Δ^9-THC and CBN, while the LEU359 residue establishes more moderate contacts with all three ligands, indicating a lower-energy interaction. Residues LEU193 and VAL196 demonstrate exclusive specificity for the cannabinoid CBD, likely attributed to the greater conformational flexibility of the species conferred by the linkage between the phenolic ring and the methylcyclohexene, indicating that this ligand seeks distinct conformations in the orthosteric site. Less frequent interactions are observed with the PHE268 residue for the cannabinoids CBN and CBD, suggesting occasional contacts that may contribute to the secondary stabilization of the complex. These interactions reveal a standard molecular recognition mechanism for the alkyl chains of cannabinoids, with specific variations that may influence the affinity and selectivity of binding to the CB1 receptor.

The results of hydrophobic interactions demonstrate that the PHE379 residue is the only conserved element in interactions with the phenolic group of the three ligands, although with notable variability in selectivity and contact frequency. For Δ^9-THC, it was observed that the PHE379 residue acts primarily to anchor the phenolic fragment. This highly targeted interaction suggests a stereospecific recognition mechanism that contributes to the high affinity characteristic of this ligand at the binding site. In contrast, the complexes with the cannabinoids CBN and CBD exhibited more distributed interaction patterns, where PHE379 participates with a 50-56% frequency in contact with the phenolic group, contributing to molecular stabilization with other hydrophobic residues. The cannabinoids Δ^9-THC and CBN share a complementary interaction profile involving the VAL196 and LEU193 residues, indicating a conserved recognition mechanism for these ligands. However, the phenol in Δ^9-THC still exhibits contact with the PHE268 residue, which is absent in the other ligands. The PHE170 residue showed selective importance in anchoring the cannabinoid CBD, reinforcing the conformational rearrangement of this more flexible ligand in the active site.

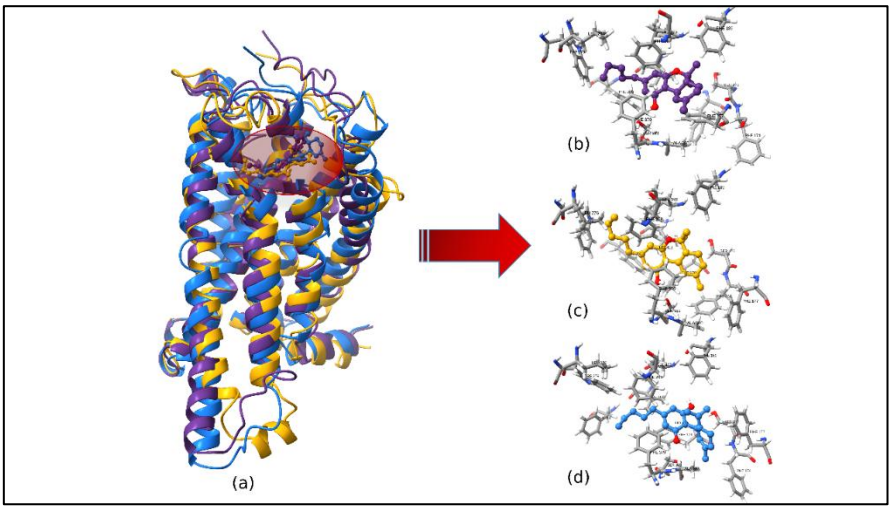

Figure 4. Ligand-receptor interaction CB1: (a) poses: Δ^9-THC (purple), CBN (yellow) and CBD (blue); (b), (c) and (d) interactions considering optimal binding energies.

As mentioned earlier, ring A, represented by a cyclohexene ring in the cannabinoids Δ^9-THC and CBD and by a benzene ring in CBN, exhibits remarkable variability in its hydrophobic interaction patterns with the active site of the CB1 receptor. Despite this conformational diversity, residues PHE174 and PHE177 emerge as conserved anchoring points, establishing significant contacts with ring A of the three ligands. Residue PHE268 presents a more diffuse distribution of interactions, but contributes energetically to the stabilization of the complexes, as evidenced by the data in Table 1. Residue ALA380 stands out as a highly selective hydrophobic contact for the cannabinoid CBD. This interaction is facilitated by the flexibility of the σ linkage between the phenolic ring and the cyclohexene ring of this cannabinoid's structure, which allows the aliphatic portion to approach the side chain of residue ALA380. Although residue ALA380 also interacts sporadically with the cannabinoids Δ^9-THC and CBN, such contacts are highly selective, occurring exclusively with the fragment corresponding to ring A of these ligands.

Table 1. Interaction energies (kcal/mol) of the cannabinoids Δ^9-THC, CBN, and CBD with the main residues of the CB1 receptor.

Residues	Cannabinoids					
	Δ^9–THC		CBN		CBD	
	Number of duplicates					
	1st duplicate	2nd duplicate	1st duplicate	2nd duplicate	1st duplicate	2nd duplicate
TRP279	–2.16±0.678	–2.72±0.738	–1.33±0.510	–2.56±1.08	–2.70±0.825	–1.40±0.498
PHE200	–1.53±0.502	–1.63±0.552	–1.50±0.552	–2.30±0.677	–1.06±0.614	–1.53±0.835
LEU276	–1.47±0.537	–0.808±0.422	–1.14±0.499	–0.826±0.526	–1.43±0.648	–0.633±0.583
LEU193	–3.90±0.783	–4.57±1.17	–3.89±1.06	–3.71±1.32	–2.35±0.867	–2.18±0.923
VAL196	–3.12±0.726	–3.24±0.796	–3.01±0.675	–3.53±0.934	–1.52±0.600	–1.72±0.761
PHE379	–4.71±0.916	–4.69±1.06	–4.06±1.14	–4.53±0.992	–2.14±0.982	–2.81±1.27
PHE268	–4.07±0.882	–3.84±0.833	–2.80±0.916	–3.58±0.786	–3.65±1.06	–3.14±1.08
PHE170	–2.27±1.842	–3.78±0.669	–4.72±0.696	–3.28±1.24	–3.33±0.96	–3.89±1.07
PHE174	–2.06±1.78	–3.40±0.774	–4.15±0.825	–2.96±1.01	–3.89±0.825	–3.15±1.47
PHE177	–2.97±1.32	–2.22±0.554	–1.49±0.667	–1.65±0.915	–3.58±0.842	–3.00±0.738
ALA380	–1.33±0.447	–1.41±0.517	–0.726±0.368	–0.814±0.518	–0.944±0,538	–1.12±0.876
ILE267	–0.817±0.418	–0.484±0.498	–0.286±0.434	–0.259±0.282	–1.98±0.945	–0.002±0.384
PHE189	–2.02±0.687	–2.38±0.686	–2.59±0.819	–1.14±0.561	–1.45±0.661	–2.07±0.843
MET384	–0.376±0.193	–0.173±0.258	–0.012±0.179	–0.105±0.150	–0.469±0.467	–0.173±0.258

Residue ILE267 establishes preferential contact with the methyl group of the cyclohexene ring of Δ^9-THC, while for the cannabinoids CBN and CBD this is less present. In the latter two cases, when interaction occurs, it is predominantly with ring A itself. Residue PHE189 exhibits a marked affinity for the benzene ring of the cannabinoid CBN, suggesting the formation of a π-stacking interaction, compatible with the aromatic nature of this fragment. As for residue PHE379, it does not significantly participate in the anchoring of the cyclohexene ring of Δ^9-THC; however, it partially contributes to the stabilization of the cannabinoids CBN and CBD, although its hydrophobic contacts in these cases are distributed between ring A and the phenolic ring. In the cannabinoid CBD, the interaction of PHE379 with the phenolic group is dominant and essential for the overall anchoring of the molecule. The MET384 residue also adapts its conformation to establish a specific hydrophobic contact with the methyl group of the cyclohexene ring, which, in turn, is not observed in a relevant way with Δ^9-THC or CBN, and its occurrence in the cannabinoid CBD is directly attributed to the greater conformational flexibility of this ligand, which allows the exploitation of alternative subpockets of the active site.

3.2.1 Interaction Energies (kcal/mol) of the cannabinoids Δ^9-THC, CBN, and CBD with the Major Residues of the CB1 Receptor

The energetic characterization of molecular interactions between the cannabinoids Δ^9-THC, CBN, and CBD and the active site of the CB1 receptor revealed a distinct pattern of hydrophobic contributions. Thermodynamic decomposition demonstrated that the alkyl chains of the ligands establish interactions predominantly mediated by van der Waals forces with conserved residues of the orthosteric pocket. Table 1 shows the interaction energies (kcal/mol) of the cannabinoids Δ^9-THC, CBN, and CBD with the main residues of the CB1 receptor. According to this table, the TRP279 residue emerges as the main contributor to energetic stabilization, being positioned as a primary hydrophobic anchor in the molecular recognition mechanism. The same table shows the PHE200 residue presenting an intermediate energetic contribution, acting as a coadjuvant element in the stabilization of the complex, and the LEU276 residue showing lower energetic magnitude, but exhibiting greater conformational variability between replicates, thus suggesting the role of a flexible modulator of the interactions. Furthermore, comparative analysis reveals distinct patterns of molecular specificity: while Δ^9-THC shows greater stabilization with the LEU276 residue, the cannabinoid CBD exhibits the greatest energy range with the TRP279 residue, indicating specific conformational adaptations. The results establish a well-defined energy hierarchy, in which the TRP279 residue acts as a primary anchoring site, the PHE200 residue provides complementary

stabilization, and the LEU276 residue functions as a modulator of conformational flexibility. The stabilization of cannabinoids by the TRP279 residue, which has a binuclear aromatic system (indol-benzene), is mainly caused by the attractive interaction between the electron-rich π system (donor) of the aromatic ring of tryptophan and the σ* orbital (acceptor) of the C-H bonds of the terminal alkyl tail (C-H•••π interaction).

According to Table 1, residues LEU193 and VAL196 show frequent interactions with the alkyl chain of CBD, exhibiting temporal occupancy of 60% to 81% during MD simulations. Energy analysis revealed significant contributions of these residues to the stabilization of the complex, and the results indicate that residues LEU193 and VAL196 play an important role in positioning the alkyl chain of the cannabinoid CBD within the hydrophobic channel of the CB1 receptor. The magnitude of the interaction energies, particularly for residue LEU193, which approaches the stabilization provided by residue TRP279, suggests that they constitute key elements in the molecular specificity of the cannabinoid CBD. Less important residues such as ILE280 and LEU359 do not show significant interaction energies.

In general, all residues that establish hydrophobic contacts with the phenolic ring exhibit favorable interaction energies, although with significant variations between ligands. As discussed earlier, the PHE379 residue acts as a primary anchor in the stabilization of Δ^9-THC through highly favorable interactions with its phenolic ring (Table 1). For CBN, the energies remain robust, indicating a similar recognition mode between these two structurally related ligands. In the case of the cannabinoid CBD, the interaction energy with the PHE379 residue is drastically reduced, suggesting that, due to its greater flexibility, this cannabinoid experiences distinct orientations in the active site, in which the phenolic ring is not the main anchoring determinant. This pattern is corroborated by the interaction energies with the VAL196 and LEU193 residues, which also show significantly weaker values for the cannabinoid CBD, compared to the cannabinoids Δ^9-THC and CBN. These results reinforce the hypothesis that these residues play a secondary role in stabilizing the cannabinoid CBD at the active site. Residues PHE268 and PHE170 exhibit more homogeneous energy profiles among the three cannabinoids. However, the role of residue PHE170 in the recognition of the cannabinoid CBD stands out, with energies comparable to those observed for the cannabinoids Δ^9-THC and CBN, suggesting that this residue may act as an alternative anchoring point for the cannabinoid CBD. Although residue PHE379 shows the highest frequency of contact with the phenolic ring and is crucial for the anchoring of Δ^9-THC, the other residues interact in a more distributed manner with other fragments of the ligands.

It is worth noting that, in the case of the Δ^9-THC and CBN residues, the interactions involving the phenolic ring exhibit significantly more favorable energies than those mediated by the alkyl chain. This difference stems from the aromatic nature of the benzene ring, whose high electron density favors more efficient interactions with the PHE379 residue of the CB1 receptor. In addition to its hydrophobic contribution, the amide group of the PHE379 residue introduces local polarity in the region adjacent to the phenolic OH group of the ligand. The energetic decomposition of this interaction reveals a substantial short-range coulombic contribution, attributed to the presence of the carbonyl group of the PHE379 residue, strongly stabilizing the interaction with the SER383 residue. Thus, the PHE379 residue plays a bifunctional role, mediating nonpolar interactions with the aromatic ring of the ligand and creating a polar microcosm that favors the formation of a specific and energetically relevant hydrogen bond with the SER383 residue. The lack of an equivalent interaction in the cannabinoid CBD likely stems from the presence of two phenolic hydroxyl groups in its structure, which compete for interactions with other polar residues in the active site, preferentially with the SER173 residue. This competition redirects the conformation of the cannabinoid CBD, preventing the formation of the specific OH•••SER383 arrangement observed in Δ^9-THC and contributing to lower affinity in the active site.

The data in Table 1 reveal that residues PHE174 and PHE177 are the main determinants of the hydrophobic stabilization of ring A, regardless of the aliphatic (Δ^9-THC and CBD) or aromatic (CBN) nature of the fragment. Residue ALA380 exhibits a slightly more favorable binding energy for Δ^9-THC, despite its contact frequency being lower with this ligand. Interestingly, although residue ALA380 shows conformational selectivity for the cyclohexene ring of CBD, resulting from the flexibility of the σ linkage between rings A and C, its interaction energy does not exceed that observed for Δ^9-THC. This apparent paradox suggests that ALA380 does not act primarily as a hydrophobic anchor, but rather as a structural component of a polar microenvironment that accommodates the phenolic OH group of cannabinoids. Indeed, the energetic decomposition of the interactions reveals that the polar contribution of the ALA380 residue is significantly more relevant in the complex with Δ^9-THC than in the complexes with cannabinoids CBN or CBD. The smaller polar component observed for the cannabinoid CBD corroborates its distance from the electron-rich subpocket formed by residues SER383, PHE379, and ALA380. This conformational rearrangement positions the cyclohexene ring of CBD in proximity to residues ALA380 and PHE170, while simultaneously displacing the opposite phenolic OH group towards a second polar subpocket, centered on residue SER173, reinforcing the evidence of competition between residues SER383 and SER173. The ILE267 residue exhibits a highly variable energetic pattern, with generally weak energies. This instability reflects the flexibility of the aliphatic side chain of the residue, which hinders the establishment of stable interactions. However, an atypical value is observed in the first duplicate with the cannabinoid CBD, attributable to the transient approximation between polar and nonpolar regions of the ligand and the residue during the first 300 ns of the simulation. After this period, the system reaches conformational equilibrium, and the energy contribution of ILE267 becomes negligible. For the PHE189 residue, the data indicate high selectivity for the benzene ring of CBN, with a more favorable average energy in the first duplicate. This interaction is compatible with π-stacking, which

confers additional stability to the CBN-CB1 complex; in contrast, for the cannabinoids Δ^9-THC and CBD, the PHE189 residue interacts preferentially with the methyl groups of the oxane ring (ring B). The interactions with the MET384 residue are consistently weak for all ligands, indicating that this residue establishes only peripheral hydrophobic contacts with the methyl group of ring A, without a significant contribution to the overall affinity.

3.2.2 Stability of Simulations of the Interactions of the cannabinoids Δ^9- THC, CBN, and CBD with the CB1 Receptor

3.2.2.1 Root Mean Square Deviation (RMSD) Analysis

Figure 5 shows the RMSD (nm) versus time (ns) profiles of residual mobility in the CB1 ligand-receptor complex. According to this figure, the cannabinoid Δ^9-THC exhibits the least conformational variation, indicating more stable behavior at the CB1 receptor binding site, achieving stability in the initial stages of the simulation, demonstrating excellent complementarity with the active site. In turn, the cannabinoid CBN exhibits greater fluctuations in the initial phase of the simulation, stabilizing only around 200 ns, and subsequently maintains satisfactory stability. The cannabinoid CBD shows partial stability between 50 and 300 ns. Nevertheless, from 300 ns onwards, the system seeks an alternate conformation, suggesting less affinity with the binding site. This instability can be attributed to the breakage of the oxane ring in its molecular structure, which confers greater conformational flexibility to the ligand.

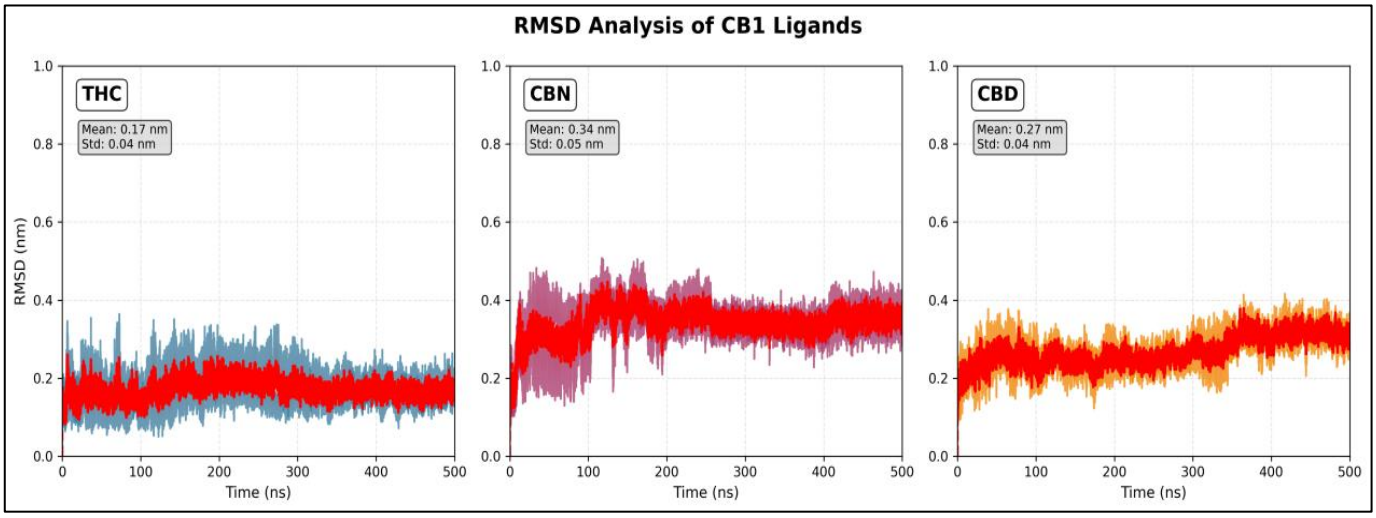

Figure 5. RMSD (nm) versus time (ns) profiles of residual mobility in the CB1 ligand-receptor complex.

3.2.2.2 Root Mean Square Fluctuation (RMSF) Profiles of Vibrational Modes in the CB1 Ligand-Receptor Complex

Figure 6 shows the RMSF (nm) versus atomic number profiles for the vibrational modes in the CB1 ligand-receptor complex. In this figure, the RMSF profiles revealed distinct patterns of residual mobility in the CB1 receptor when complexed with the cannabinoids Δ^9-THC, CBN, and CBD. Significant conformational stability was observed in the orthosteric region of the active site, evidenced by particularly low RMSF values, indicative of efficient and specific molecular coupling. In contrast, the intracellular and extracellular loop regions exhibit substantially high fluctuations, consistent with the intrinsic flexibility expected for these structural domains in G protein-coupled receptors. The remarkable quantitative similarity in the RMSF profiles among the three cannabinoid ligands strongly suggests a conserved molecular recognition mechanism in the orthosteric site of the CB1 receptor. This conformational convergence indicates that Δ^9-THC, CBN, and CBD share equivalent vibrational modes when complexed to the receptor, stabilizing in energetically favorable conformations along the simulation trajectories.

International Journal of Science and Research Methodology (IJSRM)
Volume 29, Issue 6, June 2026 ijsrm.humanjournals.com ISSN: 2454-2008

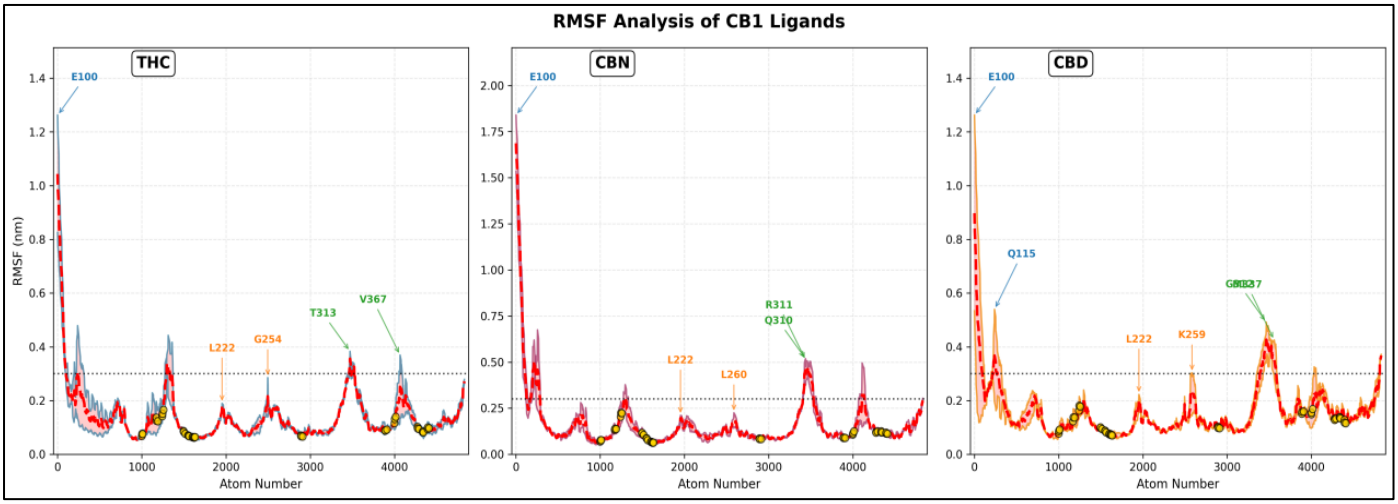

Figure 6. RMSF profiles (nm) versus atomic number of vibrational modes in the CB1 ligand-receptor complex.

3.3. Interactions of the Main Cannabinoid Fragments Δ^9-THC, CBN, and CBD with the CB2 Receptor

Figure 7 shows the ligand-CB2 receptor interactions. Figure 7a shows the analyzed poses of Δ^9-THC (purple), CBN (yellow), and CBD (blue), and Figures 7b to 7d show the interactions of the main cannabinoid fragments with the CB2 receptor. Furthermore, according to this figure, the results demonstrate that cannabinoid ligands establish highly conserved hydrophobic interactions between their alkyl chains and four key residues of the CB2 active site: TRP194, ILE186, LEU191, and MET265. These residues form a fundamental hydrophobic tunnel for the insertion and stabilization of the aliphatic tail of the hydrophobic channel, with residues TRP194, ILE186, and LEU191 showing almost exclusive specificity for the alkyl chain in all simulations. The MET265 residue participates in interactions with all ligands, although with moderate variability in intensity, suggesting an auxiliary role in the conformational adaptation of the chain end. The PHE117 residue interacts with the cannabinoids Δ^9-THC and CBN, while the contribution of this interaction is smaller for CBD. The PHE183 residue establishes secondary contacts with the alkyl chain of the three cannabinoids, suggesting a complementary importance in stabilizing the complex. These interactions reveal a standard and highly conserved mechanism of molecular recognition for the alkyl chains of cannabinoids when interacting with the CB2 receptor. The consistency of this hydrophobic core likely contributes to the common basal affinity of the three ligands, while subtle variations, especially in the contribution of PHE117 and PHE183 residues, may influence fine differences in selectivity and conformational stability at the orthosteric site of the CB2 receptor.

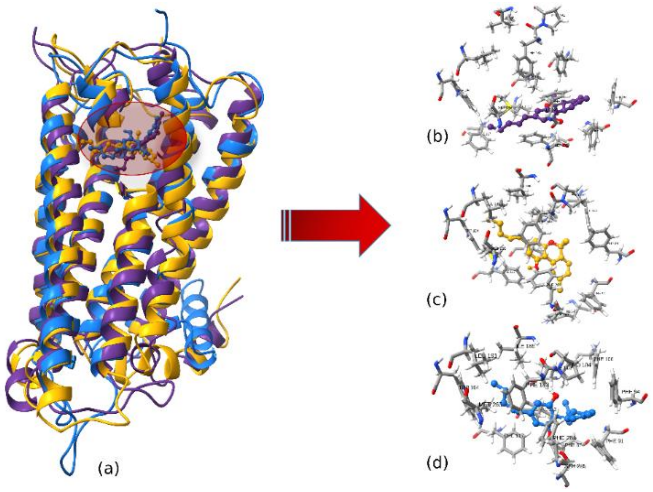

Figure 7. Ligand-CB2 receptor interaction: (a) poses: Δ^9-THC (purple), CBN (yellow) and CBD (blue); (b), (c) and (d) interactions considering the best binding energies.

The phenolic OH group of cannabinoids exhibits a more distributed and less focused interaction profile compared to other regions of the molecule. Although these contacts are often less intense in terms of fragment specificity, some residues play key roles in anchoring this group. The VAL113 residue acts as a primary anchor for the phenolic ring of Δ^9-THC and CBN. In contrast, in the

cannabinoid CBD, the VAL113 residue shows low specificity for phenol, reflecting the ability of this cannabinoid to reorient its phenolic ring due to the flexibility of the linkage between rings A and C. In this configuration, the phenol of the cannabinoid CBD preferentially interacts with residues PHE117 and PHE183, residues that act as primary anchors, while residues ILE110 and PHE281 contribute secondarily. Phenylalanines (PHE117, PHE183, and PHE281) can stabilize the complex through π–π or CH–π type interactions, especially in CBN, whose phenolic ring is part of an expanded aromatic system, and in CBD, where mobility allows for a favorable fit. Additionally, the MET265 residue appears with sporadic interactions with the phenol of CBN, but its main contribution occurs with the alkyl chain, not with the phenolic OH group.

The A ring of the studied cannabinoids exhibits partially conserved interaction patterns with the PHE91, PHE94, PHE281, and PRO184 residues of the CB2 receptor. The PHE94 residue acts as a universal anchor, establishing highly specific hydrophobic contacts with the A ring in all three ligands, reinforcing its fundamental role in the initial anchoring of this fragment to the orthosteric site. The predominant interactions involve σ(C–H)•••π type contacts, mediated by the hydrogen atoms of the cyclohexene ring (including the methyl group in CBN) and the aromatic systems of the phenylalanines. In the cannabinoid CBD, the PRO184 residue plays an essential role, where the hydrophobic contact between its aliphatic side chain and the methyl group of the cyclohexene ring induces the approximation between the second phenolic hydroxyl group and the oxygen of the peptide carbonyl group of this residue, suggesting a weak but functional hydrogen bond. This localized polar interaction, combined with the hydrophobic fit, induces a favorable repositioning of the CBD cannabinoid A ring, maximizing its complementarity with the pocket. The PHE91 residue, although present in the interactions with the A ring of all ligands, shows greater relevance for CBN, where its high specificity and the aromatic nature of the A ring favor π–π stacking interactions, contributing significantly to the stability of the complex. The PHE281 residue exhibits conformational malleability, indicating a more adaptive than structural role, rather than a primary anchor, suggesting it may act as a conformational modulator between phenol and the A ring. The PHE106 residue interacts reasonably well with the A ring of Δ^9-THC and CBD, but not with CBN, suggesting that aromatization of the A ring in the latter promotes a thermodynamically more favorable arrangement with other aromatic residues (such as PHE91 and PHE94). Residues VAL86 and PHE87 establish sporadic contacts with ring A of CBN, with PHE87 likely contributing via CH–π interactions between its aromatic ring and the methyl groups of the aromatized ring A.

Interactions with the CH_3 branches at C6 of cannabinoids involve conserved contacts with residues ILE110, PHE106, and PHE87. PHE106 shows selectivity for these branches in CBN, as PHE87 does, which shows considerable selectivity for the same fragments in the cannabinoid CBD. These interactions reveal that the region acts as a conformational integration module in the CB2 receptor, with a conserved core complemented by adaptive residues that reflect the structural differences between the cannabinoids Δ^9-THC, CBN, and CBD, contributing to molecular selectivity at the orthosteric site.

3.3.1 Interaction Energies (kcal/mol) of the cannabinoids Δ^9-THC, CBN, and CBD with the Major Residues of the CB2 Receptor

Table 2 shows the interaction energies (kcal/mol) of the cannabinoids Δ^9-THC, CBN, and CBD with the main residues of the CB2 receptor. According to this table, the energy breakdown of the interactions involving the alkyl chain of these cannabinoids reveals that residue PHE183 presents the most intense contributions to the system. However, this high stabilization is not exclusively due to the aliphatic tail; contact data indicate that PHE183 interacts bidirectionally, with a significant portion of its anchoring directed to the phenolic ring. This ability to simultaneously stabilize two distinct fragments likely explains its globally more favorable binding energy compared to other residues. Nevertheless, residues TRP194 and ILE186 stand out as the main ones responsible for the specific anchoring of the alkyl tail in the hydrophobic tunnel of the CB2 receptor. Residue TRP194 exhibits consistently strong energies and almost exclusive contact with the aliphatic chain, consolidating its role as a primary anchor. The ILE186 residue, although with more variable energy, also binds predominantly to the aliphatic tail, reinforcing the stability of the complex. The PHE117, LEU191, and MET265 residues play secondary roles in stabilizing the alkyl chain, with more modest binding energies. The LEU191 and MET265 residues, despite their limited energy contributions, exhibit high contact specificity with the alkyl chain, suggesting a structural function in the formation of the hydrophobic channel. The PHE117 residue exhibits a mixed fragmental profile, where its interaction is distributed between the phenolic ring and the alkyl chain, with greater stability in the cannabinoid CBN, moderate in Δ^9-THC, and weak in the cannabinoid CBD, reflecting the influence of the aromaticity and orientation of the C ring on its stabilizing capacity. These results indicate that, although the recognition of the alkyl chain is mediated by a conserved core of hydrophobic residues, the magnitude of energy stabilization is amplified by residues with the ability to interact with multiple fragments, such as PHE183 and, in certain contexts, PHE117.

Table 2. Interaction energies (kcal/mol) of the cannabinoids Δ^9-THC, CBN, and CBD with the main residues of the CB2 receptor.

Residues	Cannabinoids					
	Δ^9–THC		CBN		CBD	
	Number of duplicates					
	1st duplicate	2nd duplicate	1st duplicate	2nd duplicate	1st duplicate	2nd duplicate
TRP194	-2.68±0.636	-2.00±0.943	-3.51± 0.744	-2.75± 0.769	-3.01±0.733	-3.12±0.708
PHE117	-1.43±0.583	-1.14±0.810	-4.74±0.764	-1.59±0.645	-1.35±0.714	-0.764±0.667
LEU191	-0.904±0.391	-0.710±0.628	-1.49±0.564	-0.981±0.401	-1.01±0.466	-1.24±0.511
LEU182	-0.654±0.426	-0.160±0.518	-0.160±0.344	0.196±0.366	-0.388±0,359	-0.440±0.346
VAL185	-0.347±0.237	-0.021±0.080	-0.076±0.257	0.038±0.287	-0.258±0.300	-0.199±0.278
PHE281	-1.78±0.687	-4.36±3.02	-1.76±1.18	-2.82±1.26	-2.28±0.767	-1.97±0.731
PHE183	-4.48±0.977	-3.35±2.03	-4.74±0.764	-3.79±0.901	-4.70±1.34	-5.97±1.23
PHE87	-3.47±0.940	-4.69±1.90	-2.71±1.30	-3.52±0.935	-2.05±0.886	-1.96±0.717
PHE91	-1.95±1.00	-3.03±1.19	-2.21±0.873	-3.74±1.17	-2.88±0.841	-2.558±0.839
PHE94	-2.11±0.595	-1.96±0.582	-2.71±1.30	-1.81±0.676	-2.92±0.588	-3.03±0.589
ALA282	-0.104±0.249	-0.231±0.736	-0.133±0.207	-0.222±0.423	-0.194±0,232	-0.038±0.222
ILE186	-1.90±0.534	-0.331±0.455	-1.47±1.05	-1.50±0.629	-1.81±0.454	-2.04±0.526
PHE106	-1.64±0.576	-2.06±0.704	-1.29±0.636	-1.68±0.802	-1.97±0.760	-2.29±0.807
MET265	-0.681±0.423	-1.51±0.790	-1.08±0.604	-1.11±0.475	-0.795±0.405	-1.08±0.568
VAL113	-3.28±0.647	-3.15±0.758	-4.52±1.01	-2.99±0.721	-2.92±0.818	-2.41±0.987
ILE110	-4.72±0.887	-4.18±0.974	-3.33±0.986	-4.73±1.09	-2.80±0.687	-3.21±0.690
PRO184	-3.86±1.25	-0.147±0.374	-0.432±0.500	-2.18±1.94	-3.35±0.767	-4.06±1.23
VAL86	-0.542±0.306	-0.866±0.354	-1.47±1.05	-0.41±0.362	0.151±0.298	0.102±0.283
SER90	-1.71±0.622	-1.66±0.663	-1.25±0.873	-2.23±0.829	-3.35±1.11	-3.26±0.839
TRH114	-2.31±0.510	-1.64±0.722	-2.60±0.666	-2.29±0.587	-1.81±0.871	-1.86±0.751
PHE91	-1.95±1.00	-3.03±1.19	-2.21±0.873	-3.74±1.17	-2.88±0.841	-2.56±0.839
TYR25	-1.42±0.669	-0.381±0.540	-0.011±0.324	-0.32±0.512	-0.631±0.601	-1.09±0.533
HIS95	-2.73±1.13	-0.178±0.658	-1.21±0.772	-0.569±0.686	-2.09±0.912	-2.532±0.914
SER285	-0.124±0.430	-3.91±2.23	-0.286±0.531	-2.07±1.79	-0.530±1.36	0.099±0.742

As seen previously, Table 2 reveals a pattern of energy dependence of the phenolic fragment on the PHE183 residue, which acts as the main stabilizer of the phenolic group in all ligands, with consistently intense energies, reaching its most favorable value in the cannabinoid CBD. This exceptional magnitude reflects not only its proximity to the phenolic ring but also its ability to integrate interactions with multiple fragments, enhancing the overall stability of the complex. The VAL113 residue acts as a consistent phenolic anchor in Δ^9-THC and CBN, but its contribution decreases in CBD, explained by the conformational reorientation of the phenolic ring in this ligand. ILE110, which emerges for most of the simulation time near the C6 branches, provides a secondary, but important, anchoring to the phenolic fragments of the cannabinoids. The data in Table 2 quantify this interaction, revealing that ILE110 presents one of the largest favorable energy contributions for Δ^9-THC and CBN. In contrast, the smallest overall stabilizing contributions occur with CBD, most likely due to the repulsion between its second phenolic OH group and the aliphatic chain of ILE110. This specific repulsive interaction explains the less favorable energy contribution of ILE110 in the CBD complex. However, for Δ^9-THC and CBN, the intensity of the recorded energies indicates that, despite its location close to the C6 branches, this residue effectively participates in the stabilizing network of the phenolic ring, possibly through CH–π interactions involving the lateral CH_3 group of ILE110.

Regarding contacts with ring A, residues PHE91, PHE94, and PHE281 establish stable hydrophobic interactions with all three cannabinoids, although with distinct energy profiles. Residue PHE94 acts as a universal anchor, with a high contact frequency in all ligands. Its energy is particularly favorable in CBD, which aligns with the greater flexibility of the linkage between rings A and C in this ligand, allowing a tighter fit of the cyclohexene methyl group against the aromatic face of PHE94. In contrast, the less intense energies observed in the cannabinoids Δ^9-THC and CBN reflect a slightly less optimized orientation of this fragment, since there are contacts with atoms of higher electron density of nearby amino acids. PHE91 also functions as a consistent anchor of ring A, with contact frequencies and energies comparable to those of PHE94, especially in the cannabinoid CBN, where the most negative contact value of this residue with this ligand is recorded. This energy intensity is directly related to the aromatization of ring A in CBN, which favors π–π stacking interactions with phenylalanine. PHE281 exhibits a more adaptive behavior. Although it maintains contacts with ring A in all ligands, its energy varies significantly, with a notable peak in the second replicate of Δ^9-THC. This anomaly is associated with a transient π–π interaction between its aromatic ring and the phenolic ring of Δ^9-THC. In fact, in CBN and CBD, the contacts of the PHE281 residue are distributed between ring A and phenol, reinforcing its role as a conformational modulator at the interface between the two rings, and not as a primary anchor of cyclohexene. The PHE87 residue interacts

predominantly with the C6 branches in Δ^9-THC and CBD, but not with ring A. Its more intense energy in Δ^9-THC stems precisely from its proximity to the methyl groups of C6, and not from direct contact with the cyclohexene ring. The PHE106 residue establishes stable contacts with all ligands, participating in both ring A and the C6 branches. In the cannabinoid CBN, however, its interaction is concentrated almost exclusively with the C6 branches, consistent with the spatial reorganization induced by the planarity of ring A. These results indicate that these radicals in C6 are not merely coadjuvants in the cannabinoid anchoring process, but act by establishing very interesting forces in the formation of the complexes. The PRO184 residue presents a markedly ligand-dependent pattern. Although it shows sporadic contact with Δ^9-THC and CBN in some replicates, its energy is consistently favorable only in CBD. This behavior is associated with the presence of the second phenolic hydroxyl group in CBD, which allows a functional proximity to the carbonyl oxygen of the PRO184 backbone, suggesting a weak polar interaction that complements the hydrophobic fit of ring A. The VAL86 residue exhibits sparse contacts and weak energies, confirming its marginal role in anchoring ring A.

3.3.2 Stability of Simulations of the Interactions of the cannabinoids Δ^9- THC, CBN, and CBD with the CB2 Receptor

3.3.2.1 Root Mean Square Deviation (RMSD) Analysis

Figure 8 shows the RMSD (nm) versus time (ns) profiles of residual mobility in the CB2 ligand-receptor complex. In the CB2 receptor simulations, the complexes with Δ^9-THC and CBN showed greater instability compared to CBD. For Δ^9-THC, the first duplicate exhibited slightly smaller fluctuations than the second. For CBN, the first duplicate showed a pronounced RMSD peak around 180 ns, while the second remained more stable. In turn, CBD exhibited remarkably stable behavior in both duplicates, with smooth fluctuations throughout the simulation, with the overall average much lower than in the THC and CBN simulations. These results suggest that CBD has better structural complementarity with the active site of the CB2 receptor, resulting in a more rigid complex and less prone to large conformational deviations.

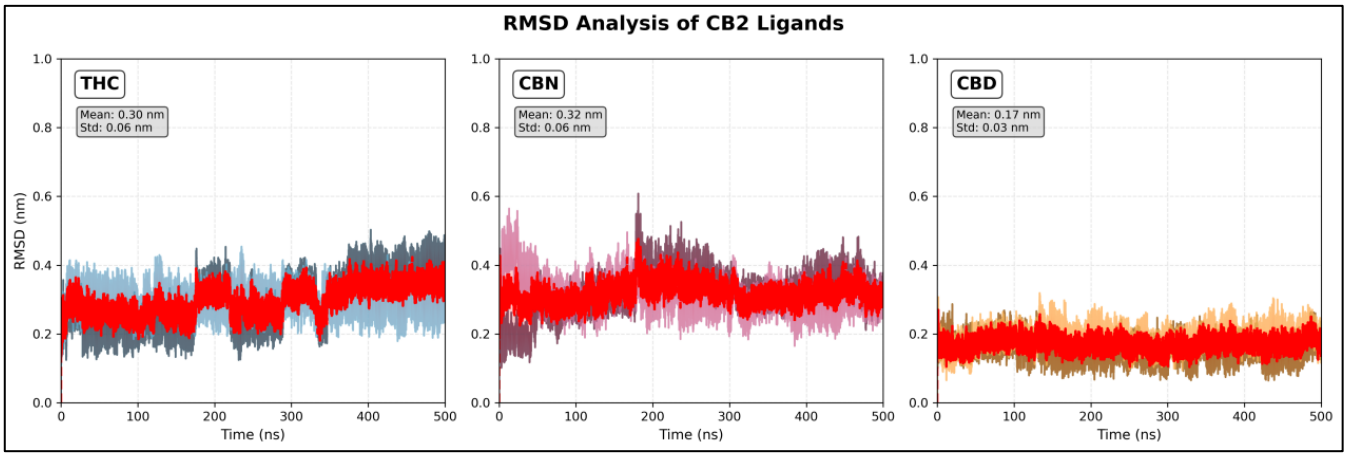

Figure 8. RMSD (nm) versus time (ns) profiles of residual mobility in the CB2 ligand-receptor complex.

3.3.2.2 Root Mean Square Fluctuation (RMSF) Profiles of Vibrational Modes in the CB2 Ligand-Receptor Complex

Figure 9 shows the RMSF (nm) versus atomic number profiles for the vibrational modes in the CB2 ligand-receptor complex. Unlike CB1, the fluctuations of CB2 when complexed with Δ^9-THC, CBN, and CBD show that the largest fluctuations occur in the intracellular loops. Marked conformational stability was observed in critical regions of the orthosteric site, evidenced by consistently low RMSF values along most residues, indicative of efficient and specific molecular coupling. In contrast, the terminal domains and certain loop segments, particularly in the regions near residues PHE21, LYS319, and GLY225, exhibited significantly high fluctuations.

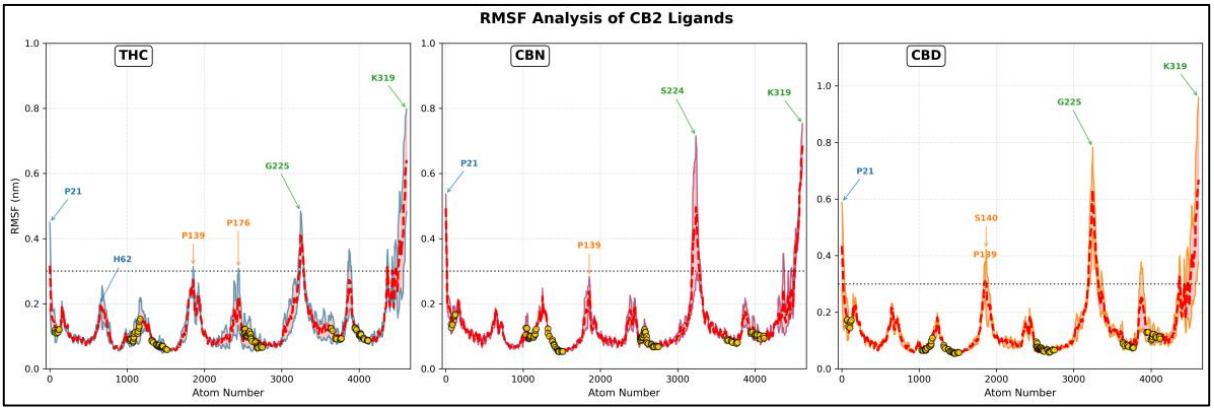

Figure 9. RMSF profiles (nm) versus atomic number of vibrational modes in the CB2 ligand-receptor complex.

The similarity in the RMSF of the three cannabinoids reinforces a conserved molecular recognition mechanism in CB2. The mobilities of residues LYS319 and G225 in all simulations suggest that these amino acids may play important roles in modulating the affinity of these cannabinoids for the CB2 receptor.

4 Concluding Remarks

The research conducted with MEP indicated the existence of key structural features of the cannabinoids Δ^9-THC, CBN, and CBD that enable interactions with CB1 and CB2 receptors and are reflected in their pharmacological properties. These features point to their relevance in reducing IOP (interaction of Δ^9-THC and CBN with the CB1 receptor) or increasing this pressure (interaction of CBD with CB1), in exerting sedative (CBN and CBD), analgesic, anti-inflammatory (CBN and CBD), and neuroprotective effects. In addition, these key structural features are also determinants of the existence (interaction of Δ^9-THC with CB1) or not (interaction of CBN and CBD with CB1) of psychoactivity in these cannabinoids.

In turn, ligand-receptor research has shed light on aspects concerning the interactions of the cannabinoids Δ^9-THC, CBN, and CBD with CB1 and CB2, and has provided insights associated with the pharmacological properties of cannabinoids in glaucomatous processes.

Acknowledgements

The authors are very grateful to the Instituto Amazônia dos Saberes (IASA-MA) and the Laboratório de Solos e Plantas (LSP) of IFPA-Castanhal for their help in preparing the manuscript, and to the Laboratório de Química Teórica e Computacional (LQTC-UFPA) and LSP-IFPA for their computational support.

The authors declare no conflict of interest.

REFERENCES

[1] Tang J, Tang Y, Yi I, Chen DF. The Role of Commensal Microflora-Induced T Cell Responses in Glaucoma Neurodegeneration. Prog. Brain Res. 2020; 256(1): 79-97.
[2] Jordan E, Nguyen GN, Piechot A, Kayser O. Cannabinoids as New Drug Candidates for the Treatment of Glaucoma. Planta Medica .2022; 88(14):1267-1274.
[3] Shan S, Wu J, Cao J, Feng Y, Luo Z, Song P, Rudan I. Global incidence and risk factors for glaucoma: A systematic review and meta-analysis of prospective studies. J Glob Health. 2024; 14:04252.
[4] PK L, Pawar RS, Katare YK, Sudheesh MS. Cannabinoids as Multitarget Drugs for the Treatment of Autoimmunity in Glaucoma. ACS Pharmacol Transl Sci. 2025; 8: 932-950.
[5] Cairns EA, Baldridge WH, Kelly ME. The Endocannabinoid System as a Therapeutic Target in Glaucoma. Neural Plast. 2016; Article ID 9364091: 1-10.
[6] Panahi Y, Manayi A, Nikan M, Vazirian M. The arguments for and against cannabinoids application in glaucomatous retinopathy. Biomed Pharmacother. 2017; 86:620-627.
[7] Somvanshi RK, Zou S, Kadhim S, Padania S, Hsu E, Kumar U. Cannabinol modulates neuroprotection and intraocular pressure: A potential multi-target therapeutic intervention for glaucoma. Biochim Biophys Acta Mol Basis Dis. 2022; 1868: 166325.
[8] Anand U, Paccheti B, Anand P, Sodergren MH. Cannabis-based medicines and pain: a review of potential synergistic and entourage effects. Pain Manag. 2021; 11(4): 395-403.

[9] Bonini SA, Premoli M, Tambaro S, Kumar A, Maccarinelli G, Memo M, Mastinu A. Cannabis sativa: A comprehensive ethnopharmacological review of a medicinal plant with a long history. J Ethnopharmacol. 2018; 227: 300–303.
[10] Mechoulam R. (ed) Cannabinoids as Therapeutic Agents. Boca Raton: CRC Press; 1986, Reissued 2019.
[11] van de Donk T, Niesters M, Kowal MA, Olofsen E, Dahan A, van Velzen M. An experimental randomized study on the analgesic effects of pharmaceutical-grade cannabis in chronic pain patients with fibromyalgia. Pain 2019; 160(4): 860-869.
[12] Tomida I, Pertwee RG, Azuara-Blanco A. Cannabinoids and glaucoma. Br J Ophthalmol. 2004; 88:708–713.
[13] Passani A, Posarelli C, Sframeli AT, Perciballi L, Pellegrini M, Guidi G, Figus M. Cannabinoids in Glaucoma Patients: The Never-Ending Story. J Clin Med. 2020; 9: 3978.
[14] Straiker AJ, Maguire G, Mackie K, Lindsey J. Localization of cannabinoid CB1 receptors in the human anterior eye and retina. Investig Ophthalmol Vis Sci. 1999; 40: 2442–2448.
[15] Lindner T, Schmidl D, Peschorn L, Pai V, Popa-Cherecheanu A, Chua J, Schmetterer L, Garhöfer G. Therapeutic Potential of Cannabinoids in Glaucoma. Pharmaceuticals. 2023; 16: 1149.
[16] Matsuda LA, Lolait SJ, Brownstein MJ, Young AC, Bonner TI. Structure of a cannabinoid receptor and functional expression of the cloned cDNA. Nature 1990; 346: 561–564.
[17] Straiker A, Stella N, Piomelli D, Mackie K, Karten HJ, Maguire G. Cannabinoid CB1 receptors and ligands in vertebrate retina: localization and function of an endogenous signaling system. Proc Natl Acad Sci USA. 1999; 96: 14565-14570.
[18] Porcella A, Maxia C, Gessa GL, Pani L. The human eye expresses high levels of CB1 cannabinoid receptor mRNA and protein. Eur J Neurosci. 2000; 12: 1123-1127.
[19] Yazulla S. Endocannabinoids in the retina: from marijuana to neuroprotection. Prog Retin Eye Res. 2008; 27: 501–526.
[20] Järvinen T, Pate DW, Laine K. Cannabinoids in the treatment of glaucoma. Pharmacol Ther. 2002; 95: 203-220.
[21] Afflitto GG, Aiello F, Scuteri D, Bagetta G, Nucci, C. CB1R, CB2R and TRPV1 expression and modulation in in vivo, animal glaucoma models: A systematic review. Biomed Pharmacother. 2022; 150: 112981.
[22] Murataeva N, Miller S, Dhopeshwarkar A, Leishman E, Daily L, Taylor X, Morton B, Lashmet M, Bradshaw H, Hillard CJ, Romero J, Straiker A. Cannabinoid CB2R receptors are upregulated with corneal injury and regulate the course of corneal wound healing. Exp Eye Res. 2019; 182: 74-84.
[23] Zhong L, Geng L, Njie Y, Feng W, Song ZH. CB2 cannabinoid receptors in trabecular meshwork cells mediate JWH015-induced enhancement of aqueous humor outflow facility. Investig Ophthalmol Vis Sci. 2005; 46: 1988-1992.
[24] Wei Y, Wang X, Wang L. Presence and regulation of cannabinoid receptors in human retinal pigment epithelial cells. Mol Vis. 2009; 15: 1243-1251.
[25] Schwitzer T, Schwan R, Angioi-Duprez K, Ingster-Moati I, Lalanne L, Giersch A, Laprevote V. The cannabinoid system and visual processing: A review on experimental findings and clinical presumptions. Eur Neuropsychopharmacol. **2015**; 25: 100-112.
[26] Schwitzer T, Schwan R, Angioi-Duprez K, Giersch A, Laprevote V. The Endocannabinoid System in the Retina: From Physiology to Practical and Therapeutic Applications. Neural Plast. 2016; Artigo ID 2916732.
[27] López EM, Tagliaferro P, Onaivi ES, López-Costa JJ. Distribution of CB2 cannabinoid receptor in adult rat retina. Synapse. 2011; 65: 388-392.
[28] Bouskila J, Javadi P, Elkrief L, Casanova C, Bouchard JF, Ptito M. A comparative analysis of the endocannabinoid system in the retina of mice, tree shrews, and monkeys. Neural Plast. 2016; Artigo ID 3127658.
[29] Kumar U, Singh S, Somvanshi RK. Role of cannabinoids in glaucoma: Lowering intraocular pressure or neuroprotection. In: Medicinal Usage of Cannabis and Cannabinoids. Preedy VR, Patel VB, Mortin CR (eds.). London: Academic Press: 2023.
[30] Haspula D, Clark MA. Cannabinoid receptors: an update on cell signaling, pathophysiological roles and therapeutic opportunities in neurological, cardiovascular, and inflammatory diseases. Int J Mol Sci. 2020; 21(20): 7693.
[31] Wang MTM, Danesh-Meyer HV. Cannabinoids and the eye. Surv Ophthalmol. 2021; 66(2): 327-45.
[32] Lopez MJ, Nataneli N. Cannabis Use for Glaucoma and Associated Pain. In: StatPearls. Treasure Island (FL): StatPearls; Last Update: June 12, 2023; 2026. Available from: https://europepmc.org/article/nbk/nbk572112.
[33] Alves P, Amaral C, Teixeira N, Correia-da-Silva G. Cannabis sativa: Much more beyond Δ9-tetrahydrocannabinol. Pharmacol Res. 2020; 157: 104822.
[34] Gould J. The cannabis crop: Cannabis is one of humanity's oldest cultivated crops. But despite its long history and many uses, hard facts on its evolution and impact on the human body are in short supply. Nature. 2015; 525: s2-s3.
[35] Górny J, Kapciak A, Forenc T, Jurek J, Pelczarska A, Hunia J, Komorowski M, Kaczorowski R, Janiszewski M. Therapeutic Potencial of Cannabinoids in Glaucoma – Hit or Myth? A Review. Qual Sport. 2024; 32: 56053. eISSN 2450-3118.
[36] Aref AA, Oh D, Moore DB. Cannnabinoids for Glaucoma. San Francisco: American Academy of Ophthalmology; December 23, 2023. Available from: https://eyewiki.org/Cannabinoids_for_Glaucoma.
[37] Zhan GL, Camras CB, Palmberg PF, Toris CB. Effects of marijuana on aqueous humor dynamics in a glaucoma patient. J Glaucoma. 2005; 14(2):175-7.
[38] Schaftenaar G, Noordik JH. Molden: a pre-and post processing program for molecular and electronic structures. J Comput-Aid Mol Des. 200; 14: 123-134.
[39] Cardoso-Filho LNC, Pinheiro JC, de Figueiredo AF, Pinheiro ACB, dos Santos MAB, Gil FS, Pizon MDG, Bitencourt HR. Computational scrutiny of psychoactive cannabinoids through molecular electrostatic potential and CB1 receptor interaction. Contrib a las Cien Soc. 2024; 17(8): e9003.

[40] Chemplus: Modular Extension to HyperChem Release 8.06**.** Molecular Modeling for Windows. Gainesvill: Hyperchem, Inc; 2008.
[41] O'Boyle NM, Banck M, James CA, Morley C, Vandermeersch T, Hutchison GR. Open Babel: an open chemical toolbox. J Cheminform. 2011; 3(33): 1-14.
[42] Frisch MJ, Trucks GW, Schlegel HB, Scuseria GE, Robb MA, Cheeseman JR, Montgomery JA, Vreven T, Kudin KN, Burant JC, Millam JM, Iyengar SS, Tomasi J, Barone V, Mennucci B, Cossi M, Scalmani G, Rega N, Petersson GA, Nakatsuji H, Hada M, Ehara M, Toyota K, Fukuda R, Hasegawa J, Ishida M, Nakajima T, Honda Y, Kitao O, Nakai H, Klene M, Li X, Knox JE, Hratchian HP, Cross JB, Bakken V, Adamo C, Jaramillo J, Gomperts R, Stratmann RE, Yazyev O, Austin AJ, Cammi R, Pomelli C, Ochterski JW, Ayala PY, Morokuma K, Voth GA, Salvador P, Dannenberg JJ, Zakrzewski VG, Dapprich S, Daniels AD, Strain MC, Farkas O, Malick DK, Rabuck AD, Raghavachari K, Foresman JB, Ortiz JV, Cui O, Baboul AG, Clifford S, Cioslowski J, Stefanov BB, Liu G, Liashenko A, Piskorz P, Komaromi I, Martin RL, Fox DJ, Keith T, Al-laham MA, Peng CY, Nanayakkara A, Challacombe M, Gill PMW, Johnson B, Chen W, Wong MW, Gonzalez C, Pople JA. Gaussian 98, Revision A.6. Pittsburg: Gaussian, Inc: 1998.
[43] Becke AD. Density-functional thermochemistry. III. The role of exact exchange. J Chem Phys. 1993; 98 (7): 5648-5652.
[44] Lee C, Yang W, Parr RG. Development of the colic-salvetti correlation-energy formula into a functional of the electron density. Phys Rev B. 1988; 37(2): 785-789.
[45] Hehre WJ, Radom L, Schleyer PvR, Pople JA. Ab Initio Molecular Theory. New York:Wiley: 986.
[46] Thomas BF, Adams IB, Mascarella SW, Martin BR, Razdan RK. Structure-ctivity analysis of anandamide analogs: relationship to a cannabinoid pharmacophore. J Med Chem. 1996; 39(2): 471-9.
[47] Politzer P, Murray JS. Electrostatics and Polarization in σ- and π-Hole Noncovalent Interactions: An Overview. Chemphyschem. 2020; 21(7): 579-588.
[48] Politzer P, Murray J. The Neglected Nuclei. Molecules. 2021; 26 (10): 2982.
[49] Flukiger P, Luthi HP, Portmann S, Weber J. Molekel. Mano: Swiss Center for Scientific Computing; 2000-2001.
[50] Berman HM, Westbrook J, Feng Z, Gilliland G, Bhat TN, Weissig H, Shindyalov IN, Bourne PE. The Protein Data Bank. Nucleic Acids Res. 2000; 28: 235-242.
[51] Thorsen TS, Kulkarni Y, Sykes DA. *et al.* Structural basis of THC analog activity at the Cannabinoid 1 receptor. Nat Commun. 2025; 16: 486.
[52] Li X, Chang H, Bouma J, de Paus LV, Mukhopadhyay P, Paloczi J, Mustafa M, van der Horst C, Kumar SS, Wu L, Yu Y, van den Berg RJBHN, Janssen APA, Lichtman A, Liu ZJ, Pacher P, van der Stelt M, Heitman LH, Hua T. Structural basis of selective cannabinoid CB_2 receptor activation. Nat. Commun. 2023; 14:1447.
[53] Meng EC, Goddard TD, Pettersen EF, Couch GS, Pearson ZJ, Morris JH, Ferrin TE. UCSF ChimeraX: Tools for structure building and analysis. Protein Sci. 2023; 32: e4792.
[54] Santos-Martins D, Solis-Vasquez L, Tillack AF, Sanner MF, Koch A, Forli S. Accelerating AutoDock4 with GPUs and Gradient-Based Local Search. J Chem Theory Comput. 2021;17(2): 1060-1073.
[55] Abraham MJ, Murtola T, Schulz R, Páll S, Smith JC, Hess B, Lindahl E. GROMACS: High performance molecular simulations through multi-level parallelism from laptops to supercomputers. Software X. 2015; 1–2: 19–25.
[56] Huang J, Rauscher S, Nawrocki G, Ran T, Feig M, de Groot BL, Grubmüller H, MacKerell AD Jr. CHARMM36m: an improved force field for folded and intrinsically disordered proteins. Nat Methods. 2017; 14(1): 71-73.
[57] Huang J, MacKerell AD Jr. CHARMM36 all-atom additive protein force field: validation based on comparison to NMR data. J Comput Chem. 2013; 34(25): 2135-45.
[58] Jo S, Kim T, Iyer VG, Im W. CHARMM-GUI: a web-based graphical user interface for CHARMM. J Comput Chem. 2009; 29(11): 1859-1865.
[59] Vanommeslaeghe K, Hatcher E, Acharya C, Kundu S, Zhong S, Shim J, Darian E, Guvench O, Lopes P, Vorobyov I, Mackerell AD Jr. CHARMM general force field: A force field for drug-like molecules compatible with the CHARMM all-atom additive biological force fields. J Comput Chem. 2010; 31(4): 671-690.
[60] Johnson BW, Strand NH, Raynak JC, Jara C, Habtegiorgis K, Hand BA, Hong S, Maloney JA. Cannabinoids in Chronic Pain Management: A Review of the History, Efficacy, Applications, and Risks. Biomedicines. 2025; 13(3): 530.

How to cite this article:
José Ciríaco Pinheiro et al. Ijsrm.Human, 2026; Vol. 29 (6): 7-22

Conflict of Interest Statement: All authors have nothing else to disclose.